Supporting Information

Activating the lattice oxygen oxidation mechanism in amorphous molybdenum cobalt oxide nanosheets for water oxidation

Xiang Wang,[ab] Congcong Xing,[ac] Zhifu Liang,[ad] Pablo Guardia,[a] Xu Han,[d] Yong Zuo,[ae] Jordi Llorca,[c] Jordi Arbiol,[df] Junshan Li[g], Andreu Cabot[af]*

[a] Catalonia Energy Research Institute - IREC, Sant Adria de Besòs, 08930 Barcelona, Spain.

[b] Department of Electronic and Biomedical Engineering, Universitat de Barcelona, 08028 Barcelona, Spain

[c] Institute of Energy Technologies, Department of Chemical Engineering and Barcelona, Research Center in Multiscale Science and Engineering, Universitat Politècnica de Catalunya, EEBE, 08019 Barcelona, Spain

[d] Catalan Institute of Nanoscience and Nanotechnology (ICN2), CSIC and BIST, Campus UAB, Bellaterra, 08193 Catalonia, Spain

[e] Istituto Italiano di Tecnologia, Via Morego 30, Genova, 16163 Italy

[f] ICREA, ICREA, 08010 Barcelona, Catalonia, Spain;

[g] Institute of Advanced Study, Chengdu University, Chengdu 610106, China

*Email: acabot@irec.cat

*Email: lijunshan@cdu.edu.cn

Experimental Section

Chemicals

Ammonium molybdate tetrahydrate ($(NH_4)_6Mo_7O_{24}\cdot 4H_2O$, 90%), cobalt nitrate hexahydrate ($Co(NO_3)_2\cdot 6H_2O$, 99.9%), potassium hydroxide (KOH, 85%), iridium(IV) oxide (IrO_2, 99.9% metal basis), and Nafion (5 wt% in a mixture of low aliphatic alcohols and water) were obtained from Sigma-Aldrich. 2-Methylimidazole ($C_4H_6N_2$, 99%) was purchased from Acros Organics. Methanol, ethanol and isopropanol were of analytical grade and obtained from various sources. Milli-Q water was obtained from a Purelab flex from Elga. All chemicals were used as received, without further purification.

Synthesis of zeolitic imidazolate framework (ZIF-67)

ZIF-67 was produced following a modified version of a previously reported procedure.[1] Typically, 0.87 g $Co(NO_3)_2\cdot 6H_2O$ was dissolved in 30 mL methanol to obtain a clear solution. Subsequently, the solution was poured into 30 mL methanol containing 1.97 g 2-methylimidazole under vigorous stirring. After mixing completely, the solution was incubated for 24 h at room temperature. Purple precipitates were collected by centrifugation, washed with methanol at least three times, and finally dried at 60 ℃ overnight.

Synthesis of Mo-Co MOFs

120 mg of as-prepared ZIF-67 powder was ultrasonically dispersed in 20 mL ethanol. The dispersion was poured into a 100 mL aqueous solution containing 50 mg, 100 mg or 200 mg of $(NH_4)_6Mo_7O_{24}\cdot 4H_2O$ under magnetic stirring. The mixture was then stirred vigorously for 12 hours at room temperature. Lavender-colored precipitates were collected by centrifugation, washed with water at least three times, and finally freeze-dried overnight. The obtained products were labelled as Mo-Co MOF-50, Mo-Co MOF-100 and Mo-Co MOF-200. The effect of stirring time was analyzed by preparing Mo-Co MOF-100 with different stirring times: 1 h, 3 h and 12 h. The effect of the Mo precursor was analyzed by replacing $(NH_4)_6Mo_7O_{24}\cdot 4H_2O$ with the equivalent molybdenum molar amount of $Na_2MoO_4\cdot 2H_2O$, to obtain a sample labelled as Na_2MoO_4-ZIF-67.

Synthesis of Co_3O_4 nanocrystals and amorphous $MoCo_xO_y$ nanosheets

ZIF-67 and Mo-Co MOF powders were annealed in a muffle furnace at 350 ℃ for 2 h with a

heating rate of 3 ℃ min^{-1} under an air atmosphere. Black products were collected after natural cooling to ambient temperature and labelled as Co_3O_4 and $MoCo_xO_y$-50, $MoCo_xO_y$-100, $MoCo_xO_y$-200, and Na_2MoO_4-$MoCo_xO_y$, depending on the MOF precursor powder used. To explore the effect of the annealing temperature, the Mo-Co MOFs-100 was also annealed at 450 ℃ and 550 ℃ for 2 h. Table S1 lists all the samples produced and tested in this study.

Material Characterizations and Electrocatalytic Evaluation

Powder X-ray diffraction (XRD) patterns were obtained on a Bruker AXS D8 Advance X-ray diffractometer with Ni-filtered (2 μm thickness) Cu-Kα radiation (λ= 1.5406 Å) operating at 40 mA and 40 kV. Scanning electron microscopy (SEM) analysis was conducted with a Zeiss Auriga microscope (Carl Zeiss, Jena, Germany) equipped with an energy-dispersive X-ray spectroscopy (EDS) detector operating at 20 kV. Transmission electron microscopy (TEM) analysis was carried out using a field emission gun FEI™ Tecnai F20 microscope at 200 kV with a point-to-point resolution of 0.19 nm. Atomic force microscopy (AFM) measurements were conducted using an AFM Multimode 8 system attached to a Nanoscope V electronic unit (Bruker). Raman spectroscopy was carried out on a confocal Raman spectrometer (Renishaw in Via Qontor) equipped with a Leica DM2700M microscope over the range of 50 to 1200 cm^{-1}. A power of the laser of 1 mW cm^{-2} was kept at all samples. X-ray photoelectron spectroscopy (XPS) analysis was carried out on a Specs system (Specs GmbH, Berlin, Germany) equipped with an Al anode XR50 source operating at 150 W and a Phoibos 150 MCD-9 detector. The pressure in the analysis chamber was kept below 10^{-7} Pa. Thermogravimetric analyses (TGA) were carried out in air atmosphere from 50 to 700 °C with a ramp of 5 °C min^{-1} using a Diamond TG/DTA Instruments (PerkinElmer, Waltham, MA). EPR spectroscopy was conducted on a Bruker EMXplus instrument (Bruker, Germany) with a microwave frequency of 9.40 GHz at 100 K.

All electrochemical measurements were performed at room temperature on a CHI760E electrochemical workstation (Shanghai Chenhua Instrument Co. Ltd., China) using a standard three-electrode cell. A graphite rod was used as the counter electrode and Hg/HgO (1.0 M KOH) as the reference electrode. Linear sweep voltammetry (LSV) was conducted at a scan rate of 5 mV s^{-1} from 0 to 1.0 V in O_2-saturated 1.0 M KOH electrolyte. All the presented data were corrected with 90% iR-compensation. Electrochemical impedance spectroscopy (EIS) analysis

was carried out in a frequency range from 100 kHz to 0.01 Hz at 5 mV and recorded at 1.55 V. The electrochemical double-layer capacitance (C_{dl}) curves were obtained by cyclic voltammetry (CV) in a non-Faradaic region (0.90–1.00 V vs. RHE) at scan rates in the range 20 to 200 mV s^{-1}. The long-term durability was tested using chronoamperometry at a constant current density of 10 mA cm^{-2} for 60 h without iR compensation, and by comparing the LSVs curves (1.2 to 1.7 V) before and after 2000 CV cycles at a scan rate of 0.2 V s^{-1}. In-situ Raman spectra were collected after different CV cycles in the range 1.3 V to 1.7 V at a scan rate of 0.01 V s^{-1} on an Xplora Plus Raman microscope (Horiba, France) with a 532 nm excitation wavelength.

Table S1. Complete list of samples produced and characterized, including name, precursors and processing conditions.

Sample name	MOF	Mo precursor	Mo precursor amount (mg)	Stirring time (h)	Annealing temperature (ºC)
ZIF-67	ZIF-67	-	-	-	-
Mo-Co MOF-50	ZIF-67	$(NH_4)_6Mo_7O_{24}{\cdot}4H_2O$	50	12	-
Mo-Co MOF-100	ZIF-67	$(NH_4)_6Mo_7O_{24}{\cdot}4H_2O$	100	12	-
Mo-Co MOF-100-1h	ZIF-67	$(NH_4)_6Mo_7O_{24}{\cdot}4H_2O$	100	1	-
Mo-Co MOF-100-3h	ZIF-67	$(NH_4)_6Mo_7O_{24}{\cdot}4H_2O$	100	3	-
Mo-Co MOF-200	ZIF-67	$(NH_4)_6Mo_7O_{24}{\cdot}4H_2O$	200	12	-
Na_2MoO_4-ZIF-67	ZIF-67	$Na_2MoO_4{\cdot}2H_2O$	140	12	
Co_3O_4	ZIF-67	-	-	-	350
$MoCo_xO_y$-50	ZIF-67	$(NH_4)_6Mo_7O_{24}{\cdot}4H_2O$	50	12	350
$MoCo_xO_y$-100	ZIF-67	$(NH_4)_6Mo_7O_{24}{\cdot}4H_2O$	100	12	350
$MoCo_xO_y$-100-450ºC	ZIF-67	$(NH_4)_6Mo_7O_{24}{\cdot}4H_2O$	100	12	450
$MoCo_xO_y$-100-550ºC	ZIF-67	$(NH_4)_6Mo_7O_{24}{\cdot}4H_2O$	100	12	550
$MoCo_xO_y$-100-1h	ZIF-67	$(NH_4)_6Mo_7O_{24}{\cdot}4H_2O$	100	1	350
$MoCo_xO_y$-100-3h	ZIF-67	$(NH_4)_6Mo_7O_{24}{\cdot}4H_2O$	100	3	350
$MoCo_xO_y$-200	ZIF-67	$(NH_4)_6Mo_7O_{24}{\cdot}4H_2O$	200	12	350
Na_2MoO_4-$MoCo_xO_y$	ZIF-67	$Na_2MoO_4{\cdot}2H_2O$	140	12	350

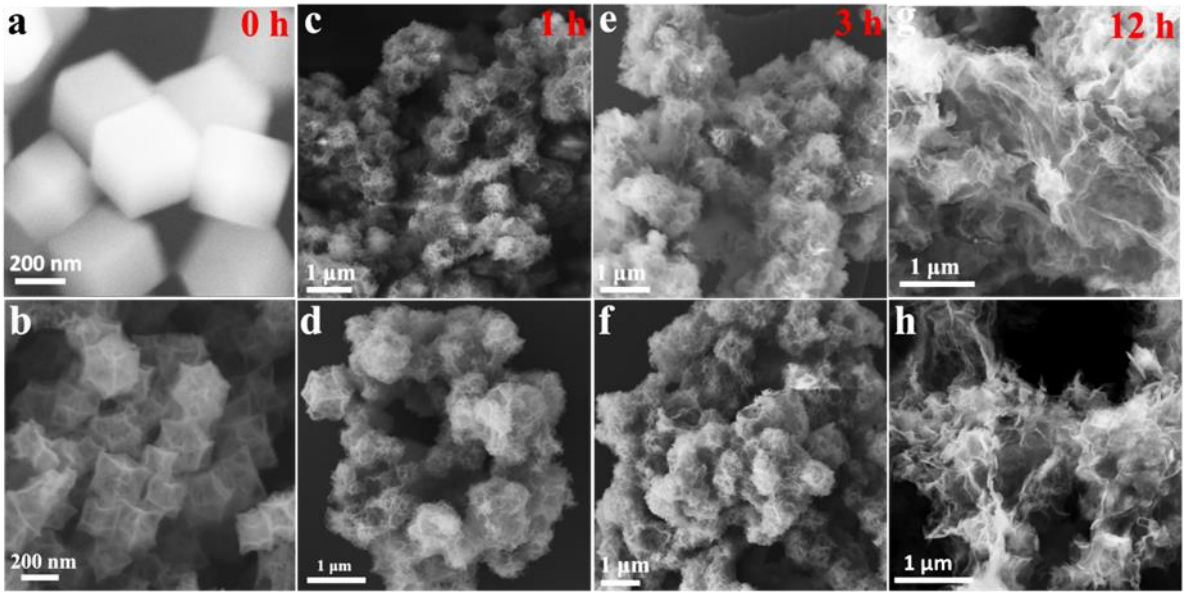

Figure S1. SEM images of a) ZIF-67, b) Co_3O_4, c) Mo-Co MOFs-1h, d) $MoCo_xO_y$-100-1h, e) Mo-Co MOFs-3h, f) $MoCo_xO_y$-100-3h, g) Mo-Co MOFs-12h, and h) $MoCo_xO_y$-100-12h.

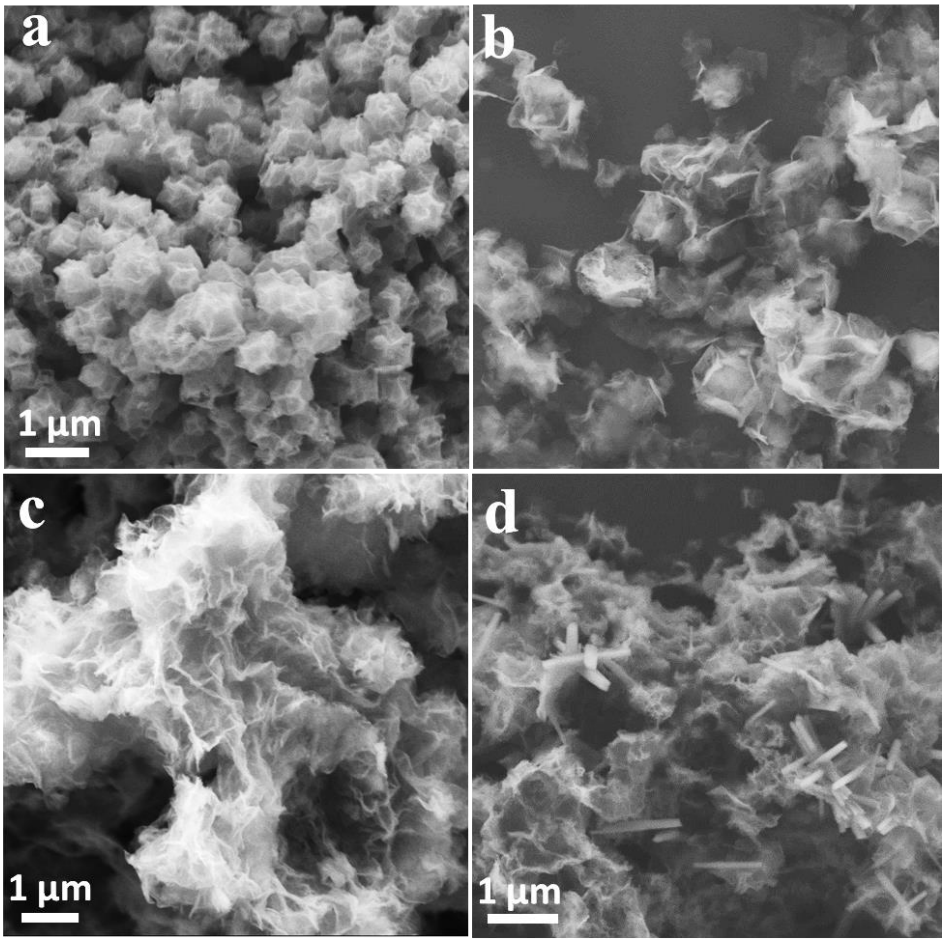

Figure S2. SEM images of a) Co_3O_4, b) $MoCo_xO_y$-50, c) $MoCo_xO_y$-100 and d) $MoCo_xO_y$-200.

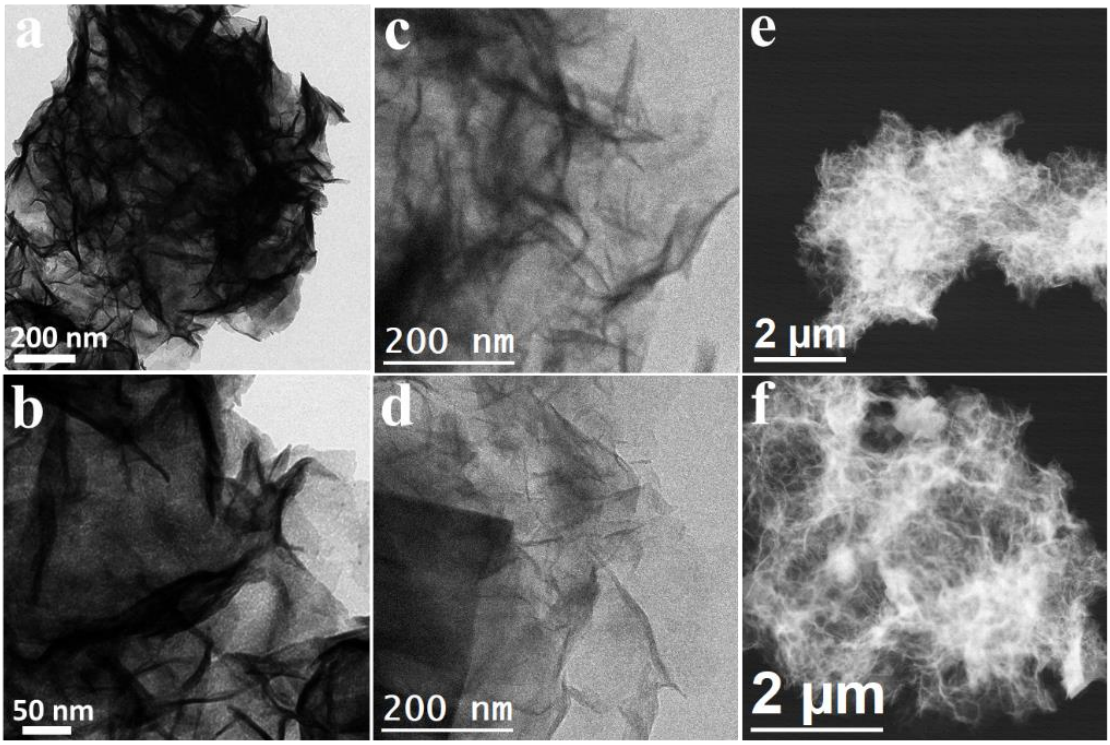

Figure S3. (a-d) TEM and (e-f) HAADF STEM images of $MoCo_xO_y$-100.

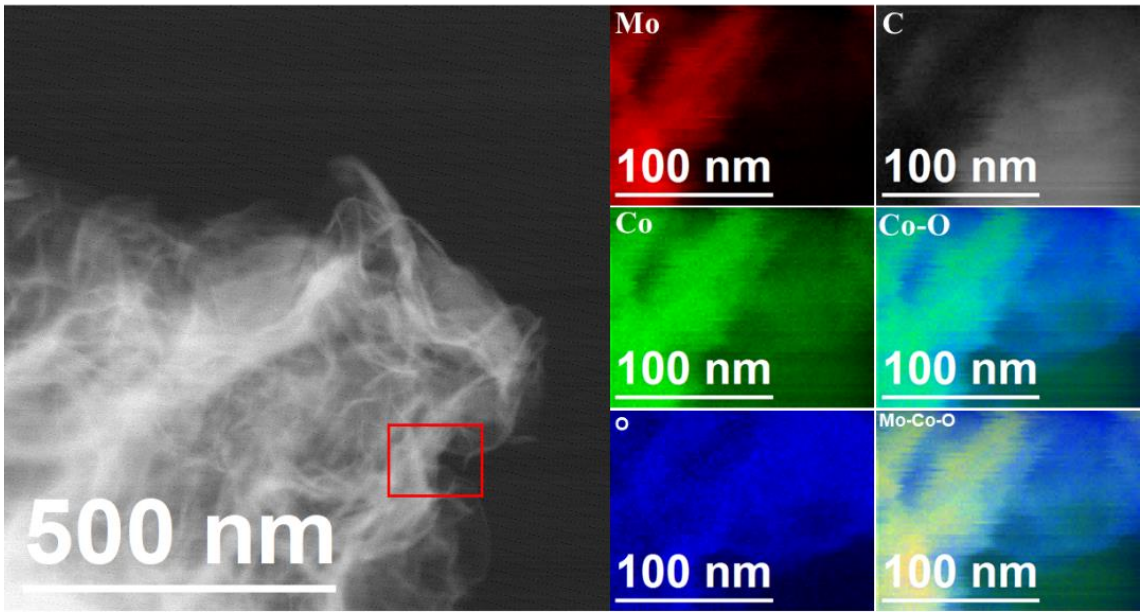

Figure. S4. EELS chemical composition maps obtained from the red squared area of the STEM micrograph of $MoCo_xO_y$-100. Individual Mo $M_{4,5}$-edges at 227 eV (red), Co $L_{2,3}$-edges at 779 eV (green), O K-edge at 532 eV and C K-edge at 284 eV (grey) and composites of Co-O and Mo-Co-O.

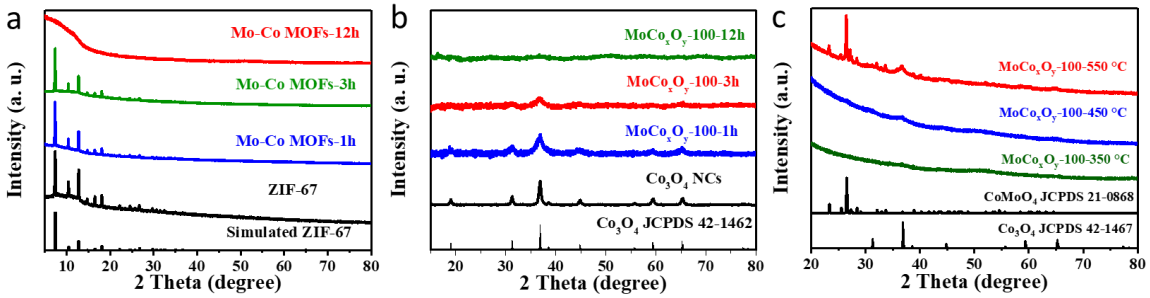

Figure S5. XRD patterns of a) Mo-Co MOFs produced using different stirring times, b) $MoCo_xO_y$-100 samples obtained from the annealing of Mo-Co MOFs produced with different stirring times and c) $MoCo_xO_y$-100 after different annealing temperature.

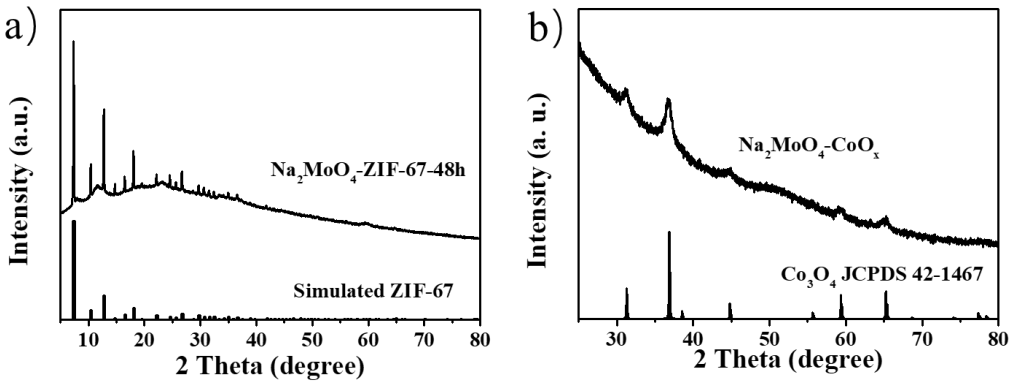

Figure S6. XRD patterns of a) Na_2MoO_4-ZIF-67 and b) Na_2MoO_4-CoO_x after 350 °C calcination.

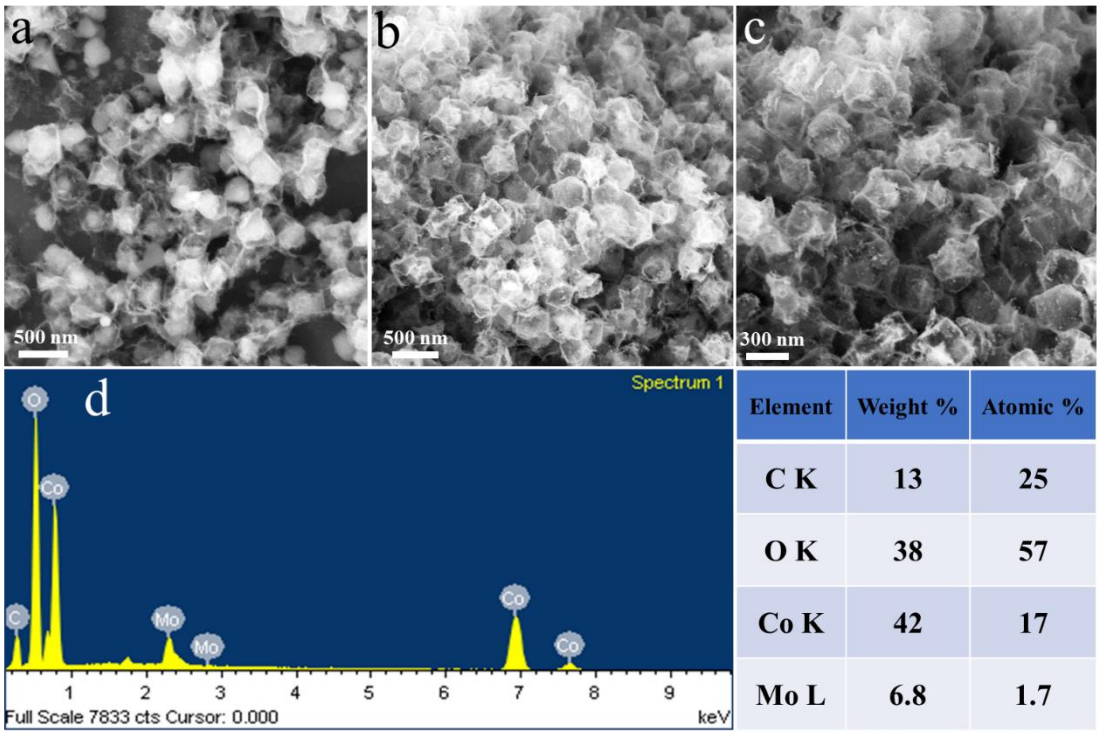

Element	Weight %	Atomic %
C K	13	25
O K	38	57
Co K	42	17
Mo L	6.8	1.7

Figure S7. a) SEM images of Na_2MoO_4-ZIF-67. b-c) SEM images and d) EDX spectrum of Na_2MoO_4-CoO_x after 350 °C calcination.

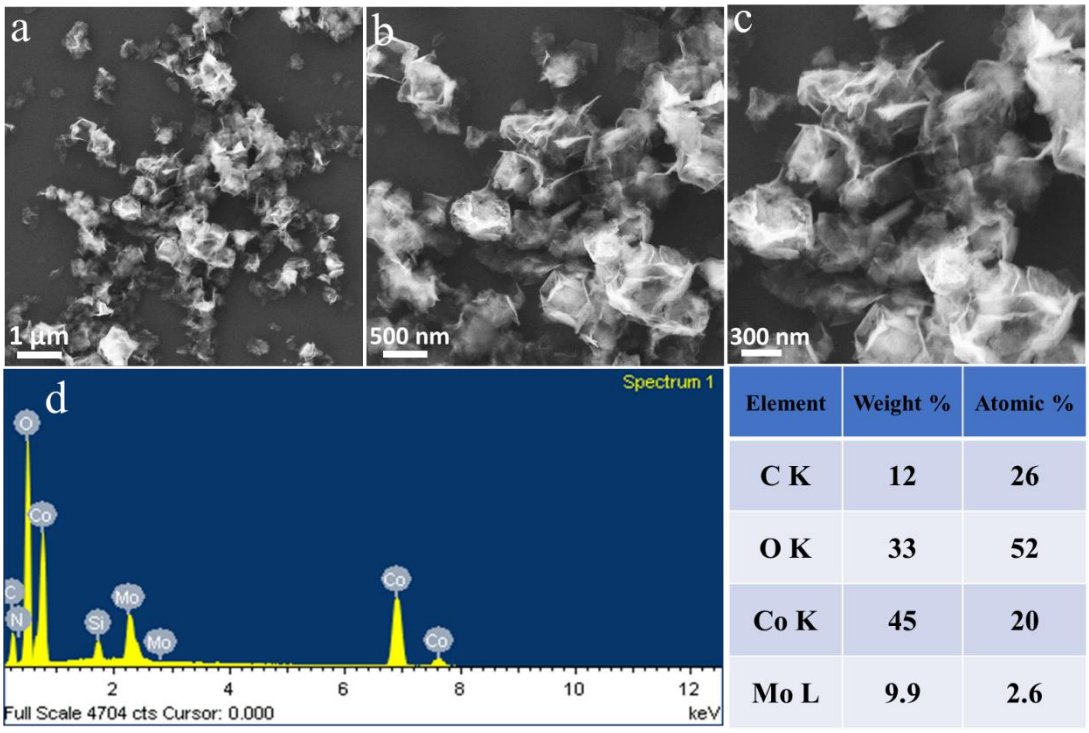

Element	Weight %	Atomic %
C K	12	26
O K	33	52
Co K	45	20
Mo L	9.9	2.6

Figure S8. a-c) SEM images and b) EDX spectrum of $MoCo_xO_y$-50 after 350 °C calcination

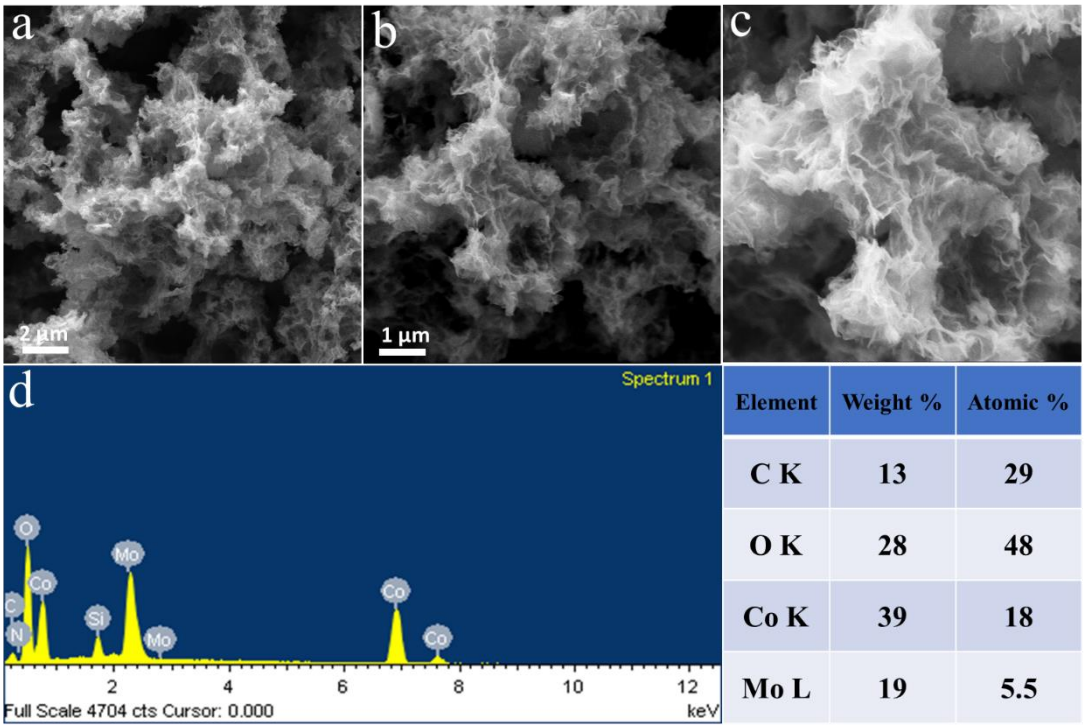

Element	Weight %	Atomic %
C K	13	29
O K	28	48
Co K	39	18
Mo L	19	5.5

Figure S9. a-c) SEM images and d) EDX spectrum of $MoCo_xO_y$-100 after 350 °C calcination

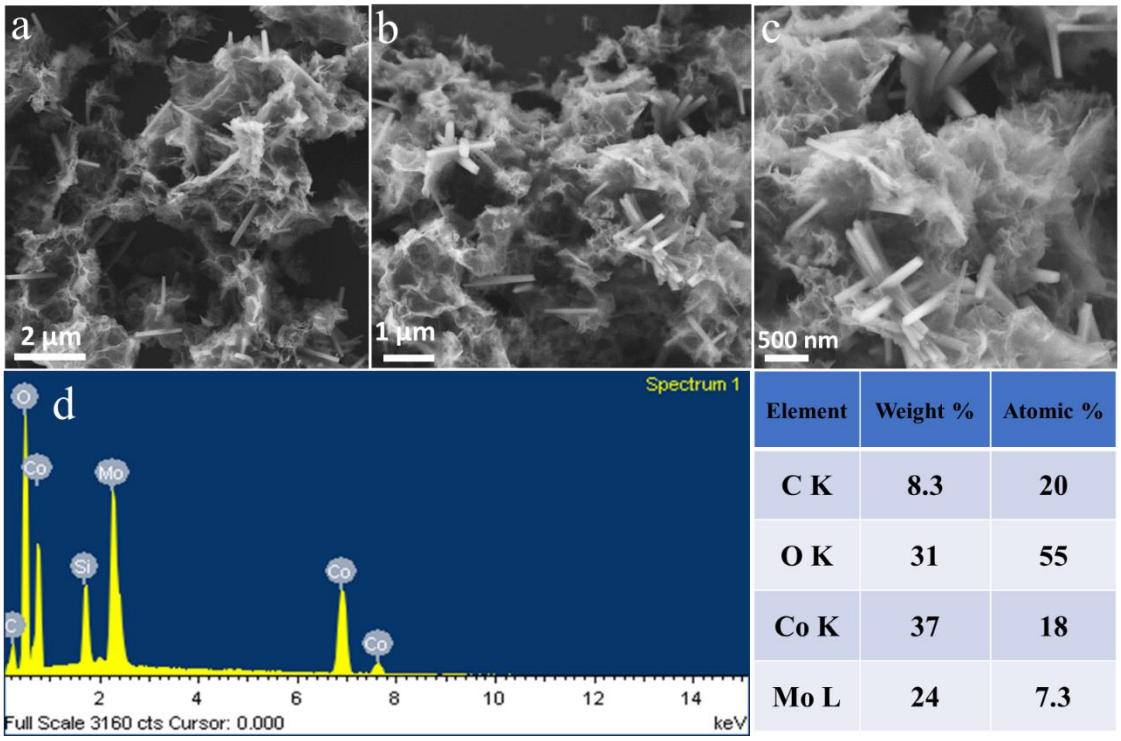

Element	Weight %	Atomic %
C K	8.3	20
O K	31	55
Co K	37	18
Mo L	24	7.3

Figure S10. a-c) SEM images and d) EDX spectrum of $MoCo_xO_y$-200 after 350 °C calcination

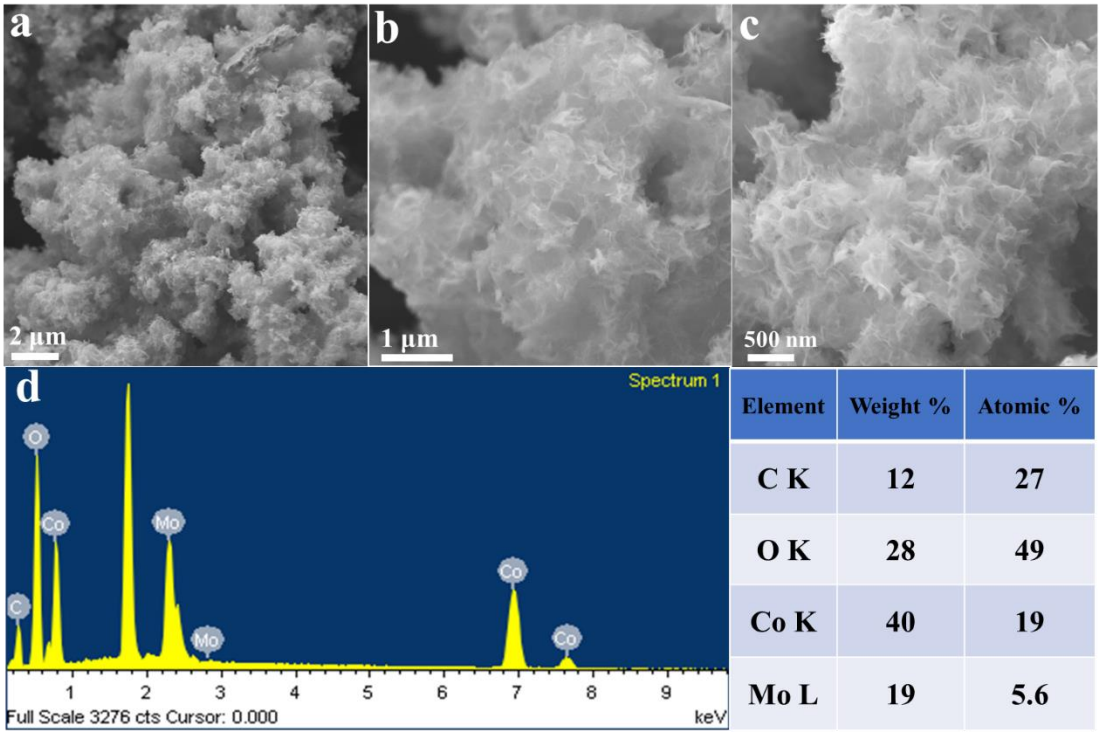

Element	Weight %	Atomic %
C K	12	27
O K	28	49
Co K	40	19
Mo L	19	5.6

Figure S11. a-c) SEM images and d) EDX spectrum of $MoCo_xO_y$-100 after 450 °C calcination

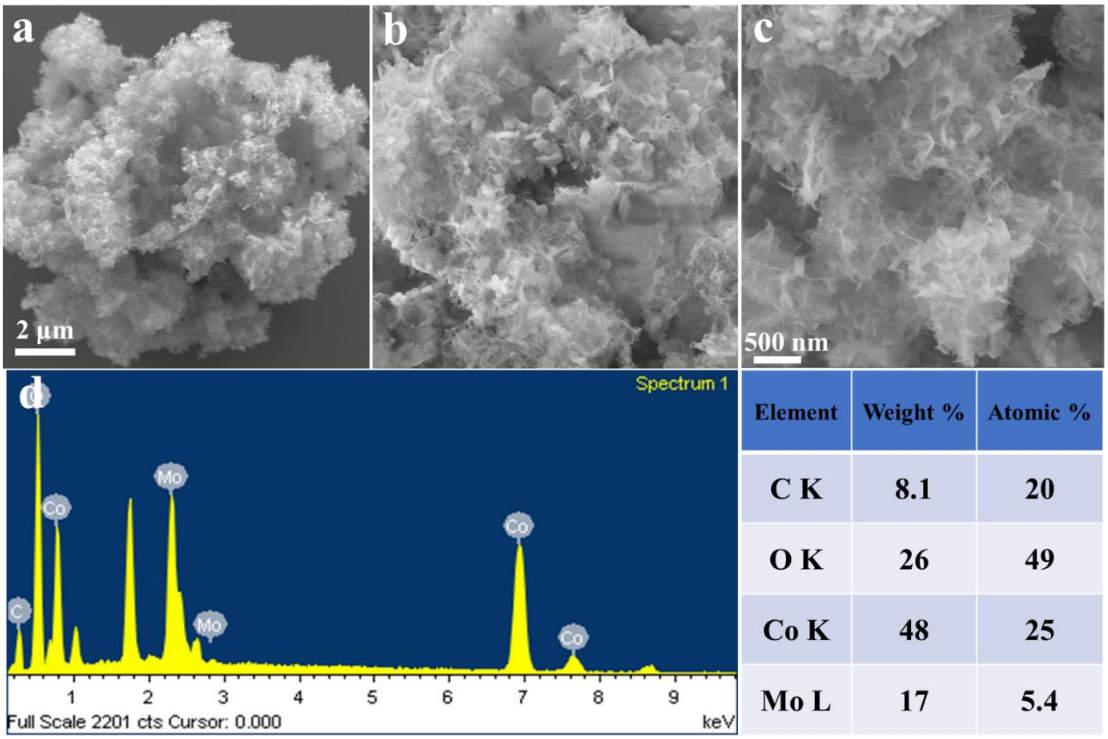

Element	Weight %	Atomic %
C K	8.1	20
O K	26	49
Co K	48	25
Mo L	17	5.4

Figure S12. a-c) SEM images and d) EDX spectrum of $MoCo_xO_y$-100 after 550 °C calcination

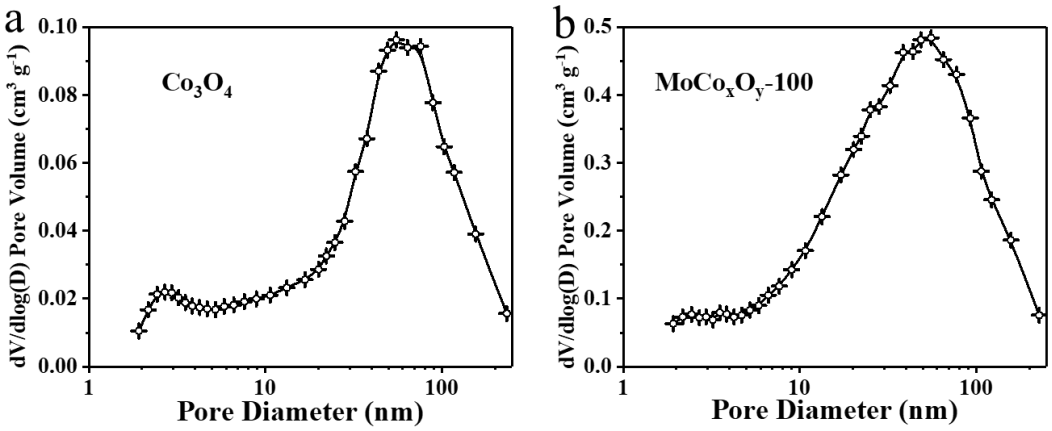

Figure S13. Pore size distribution for a) Co_3O_4 and b) $MoCo_xO_y$-100

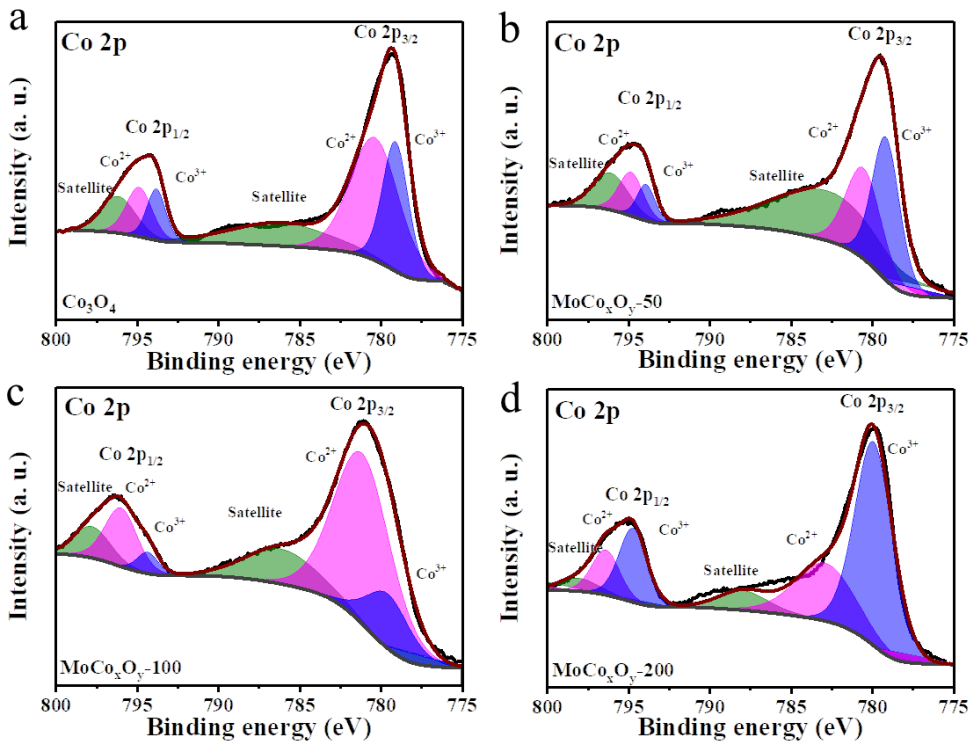

Figure S14. a-d) Co 2p high-resolution XPS spectra of Co_3O_4 and $MoCo_xO_y$ with different molybdenum contents.

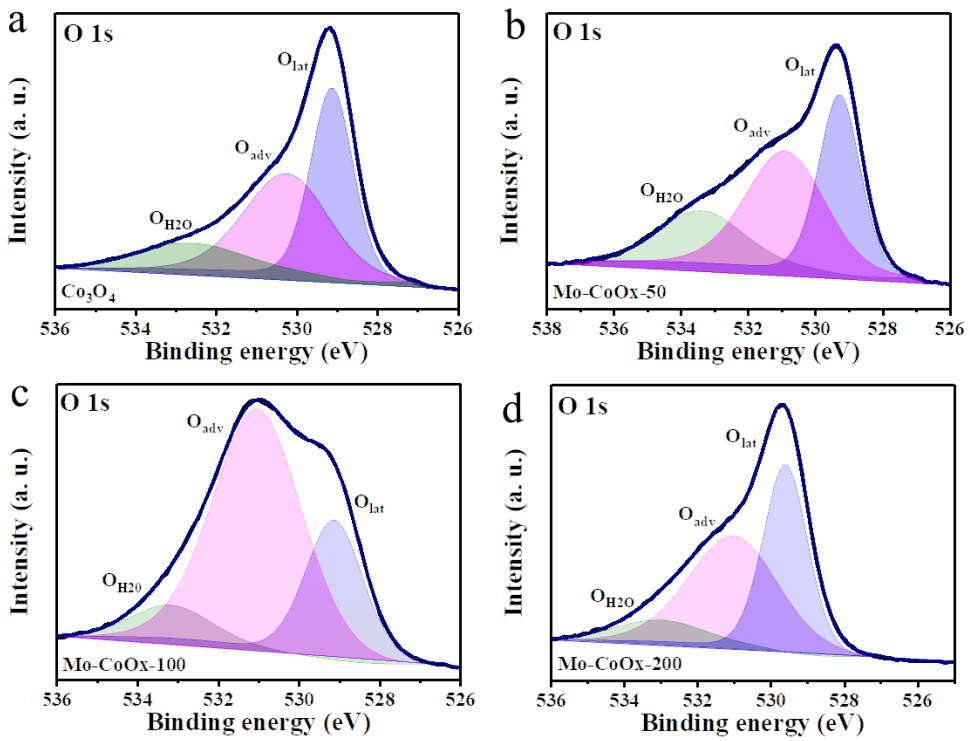

Figure S15. a-d) O 1s high-resolution XPS spectra of Co_3O_4 and $MoCo_xO_y$ with different molybdenum contents.

Table S2. Surface ratios of Co and Mo chemical states, ratio of adsorved vs. lattice oxygen, and Mo/Co ratio as obtained from the XPS analysis.

Samples	Co^{2+}/Co^{3+}	Mo^{4+}/Mo^{6+}	O_{ads}/O_{lat}	Mo/Co
Co_3O_4	3.06	-	0.62	0
$MoCo_xO_y$-50	1.96	3.3	0.66	0.21
$MoCo_xO_y$-100	0.45	0.76	1.48	0.48
$MoCo_xO_y$-200	1.33	4.2	0.56	0.29

Table S3. Comparison of OER activity of obtained catalyst.

Catalyst	η_{10} [mV]	Tafel Slope [mV dec^{-1}]
IrO_2	301	66.7
Co_3O_4	350	95.7
$MoCo_xO_y$-50	344	71.2
$MoCo_xO_y$-100	282	60.6
$MoCo_xO_y$-200	322	64.2
Co-Mo MOFs	379	109.5

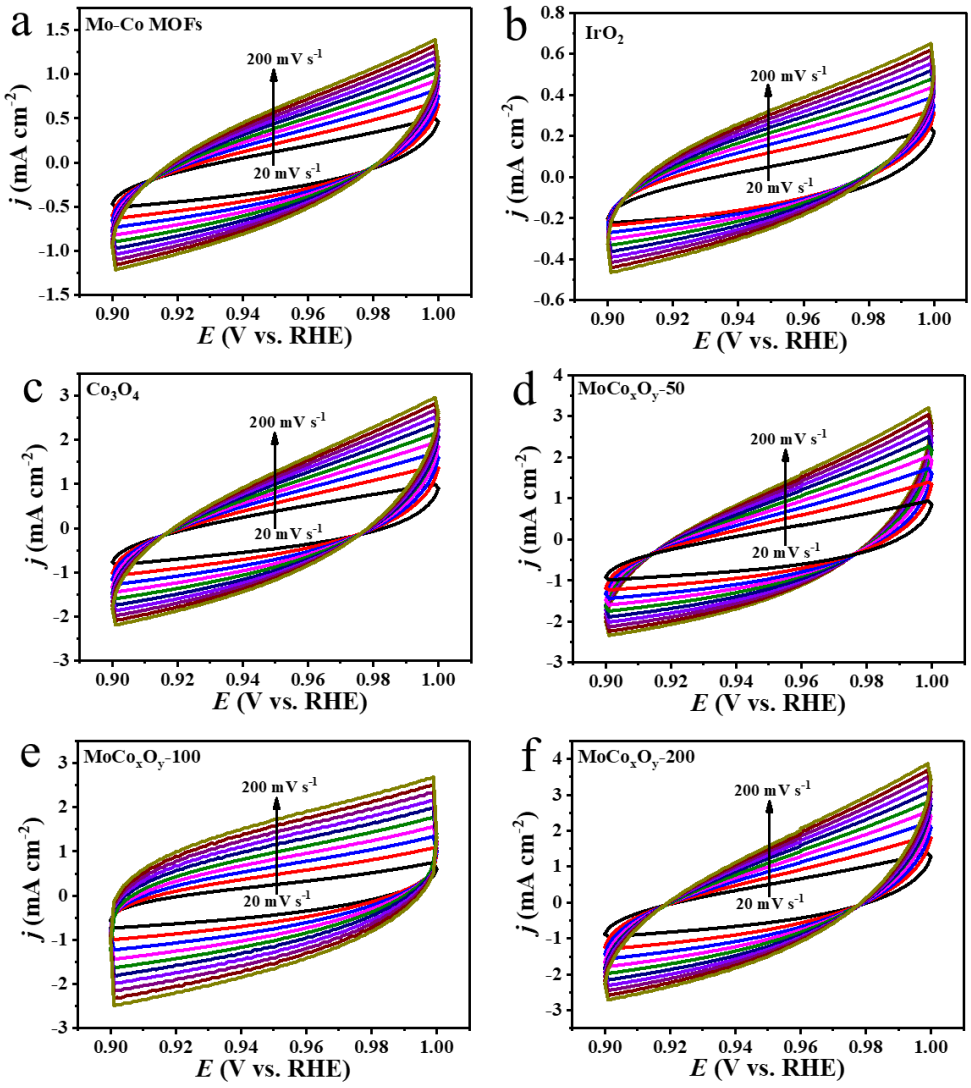

Figure S16. Cyclic voltammograms for a) Mo-Co MOFs; b) IrO_2; c) Co_3O_4 and d) $MoCo_xO_y$-50; e) $MoCo_xO_y$-100; f) $MoCo_xO_y$-200 in the non-faradaic region of 0.90-1.00 V vs. RHE at various scan rates.

Table S4. C_{dl} and ECSAs of various catalysts.

Catalyst	C_{dl} (mF cm^{-2})	ECSA (cm^{-2}) [a]
IrO_2	1.03	25.75
Co_3O_4	4.23	105.75
$MoCo_xO_y$-50	4.84	121.00
$MoCo_xO_y$-100	7.31	182.75
$MoCo_xO_y$-200	5.24	131.00
Co-Mo MOFs	2.31	57.75

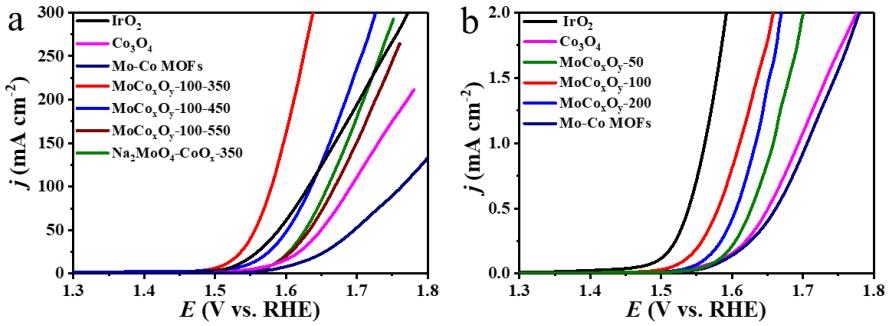

Figure S17. a) OER polarization curves for $MoCoO_x$-100 annealed at different tempratures and Na_2MoO_4-CoOx. b) ECSA-normalized OER polarization curves for Mo-Co MOFs, IrO_2, Co_3O_4, $MoCo_xO_y$-50, $MoCo_xO_y$-100 and $MoCo_xO_y$-200 in 1.0 M KOH.

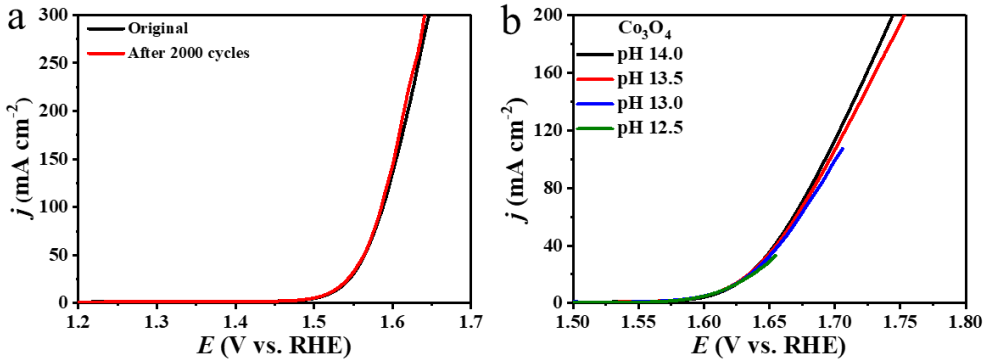

Figure S18. OER polarization curves of a) $MoCo_xO_y$-100 before and after 2000 cycles. b) Co_3O_4 at different pH values.

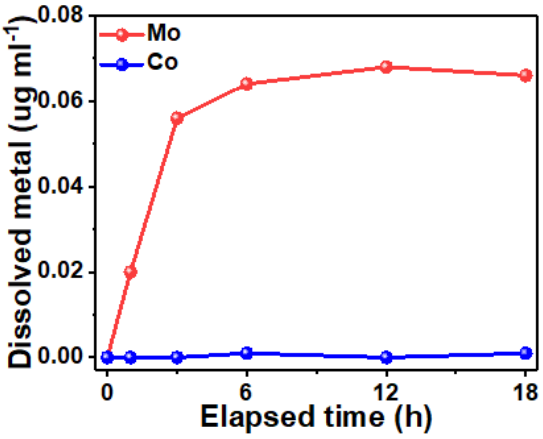

Figure S19. Time-dependent concentration of Mo and Co ions dissolved in the electrolyte during of $MoCo_xO_y$-100 a 18h chronoamperometric test at 282 mV vs. RHE

Table S5. Comparison of OER activity of amorphous $MoCo_xO_y$-100 nanosheets with recently reported Co-based electrocatalysts in alkaline electrolyte.

Catalyst	Electrolyte	Loading [mg cm^{-2}]	η_{10} [mV]	Tafel Slope [mV dec^{-1}]	References
$MoCo_xO_y$-100	1.0 M KOH	0.15	282	60.4	**This work**
A-$FeCoSeO_x$-100	1.0 M KOH	0.27	294	45.1	[2]
Co_3O_4/$CoMoO_4$-50	1.0 M KOH	0.26	318	63	[3]
Co-LDH FNSAs	1.0 M KOH	/	300	110	[4]
MoO_2-$Co_2Mo_3O_8$	1.0 M KOH	0.20	320	88	[5]
CoVS NBs	1.0 M KOH	0.30	290	78.2	[6]
$Co_2Mo_3O_8$	1.0 M KOH	0.14	290	87.5	[7]
Co_8Ag oxide	1.0 M KOH	0.12	344	48	[8]
NiCoPO/NC	1.0 M KOH	0.21	300	94	[9]
Co_3O_{4-x} HOPNPs	0.1 M KOH	/	280	73.5	[10]
CoO-MoO_2	1.0 M KOH	0.5	312	75	[11]
Co_3O_4/CoO-120s	1.0 M KOH	/	302	68.6	[12]
CoNiP-3DHFLMs	1.0 M KOH	0.13	292	98	[13]
3D CoMoOS NBs	1.0 M KOH	/	281	75.4	[14]
Co–CoO@NSC-5	1.0 M KOH	0.25	279	83	[15]
$Ni_xCo_{3-x}O_{4-y}$	1.0 M KOH	0.36	320	53	[16]

REFERENCES

1. Z.-F. Huang, J. Song, Y. Du, S. Xi, S. Dou, J. M. V. Nsanzimana, C. Wang, Z. J. Xu and X. Wang, *Nat. Energy*, 2019, **4**, 329-338.
2. Q. Qian, Y. Li, Y. Liu and G. Zhang, *Appl. Catal. B,* 2020, **266**.
3. L. Zhang, T. Mi, M. A. Ziaee, L. Liang and R. Wang, *J. Mater. Chem. A*, 2018, **6**, 1639-1647.
4. T.-J. Wang, X. Liu, Y. Li, F. Li, Z. Deng and Y. Chen, *Nano Res.,* 2019, **13**, 79-85.
5. Y. Li, H. Xu, H. Huang, C. Wang, L. Gao and T. Ma, *Chem. Commun*, 2018, **54**, 2739-2742.
6. C. Wang, H. Xu, Y. Wang, H. Shang, L. Jin, F. Ren, T. Song, J. Guo and Y. Du, *Inorg. Chem*, 2020, **59**, 11814-11822.
7. T. Ouyang, X. T. Wang, X. Q. Mai, A. N. Chen, Z. Y. Tang and Z. Q. Liu, *Angew. Chem. Int. Ed.* 2020, **59**, 11948-11957.
8. M. Yu, G. H. Moon, R. G. Castillo, S. DeBeer, C. Weidenthaler and H. Tuysuz, *Angew. Chem. Int. Ed.* 2020, **59**, 16544-16552.
9. C. Wang, W. Chen, D. Yuan, S. Qian, D. Cai, J. Jiang and S. Zhang, *Nano Energy*, 2020, **69**.
10. D. Ji, L. Fan, L. Tao, Y. Sun, M. Li, G. Yang, T. Q. Tran, S. Ramakrishna and S. Guo, *Angew. Chem. Int. Ed.* 2019, **58**, 13840-13844.
11. F. Lyu, Y. Bai, Z. Li, W. Xu, Q. Wang, J. Mao, L. Wang, X. Zhang and Y. Yin, *Adv. Funct. Mater.* 2017, **27**.
12. Z. Liu, Z. Xiao, G. Luo, R. Chen, C. L. Dong, X. Chen, J. Cen, H. Yang, Y. Wang, D. Su, Y. Li and S. Wang, *Small*, 2019, **15**, e1904903.
13. G. Li, X. Zhang, H. Zhang, C. Liao and G. Jiang, *Appl. Catal. B*, 2019, **249**, 147-154.
14. H. Xu, H. Shang, C. Wang, L. Jin, C. Chen, C. Wang and Y. Du, *Appl. Catal. B*, 2020, **265**.
15. Y. Tan, Z. Zhang, Z. Lei, W. Wu, W. Zhu, N. Cheng and S. Mu, *J. Power Sources*, 2020, **473**.
16. R. P. Antony, A. K. Satpati, K. Bhattacharyya and B. N. Jagatap, *Adv. Mater. Interfaces*, 2016, **3**.